University Of Crete

Department of Physics

Bachelor's Thesis

«Optimization of a non-linear microscope through group delay dispersion correction for two-photon excited fluorescence»

Stefanos Marinos

Table of Contents

Abstract

The purpose of this project was to optimize a laser scanning microscope powered by a femtosecond pulsed laser to acquire the best possible images of a mouse retina in different wavelengths. The chosen wavelengths correspond to different mechanisms within the sample. Such as Autofluorescence Two Photon Excited fluorescence and Second Harmonic Generation. As a result, we obtained different images depending on the wavelength emitted by the ultra-fast pulsed laser.

Introduction

Microscopy is a scientific methodology that entails the utilization of microscopes to visually examine and investigate entities that possess dimensions below the perceptible range of human vision. It serves as an essential component in several scientific fields, enabling the examination of complex characteristics pertaining to microscopic structures, cells, tissues, and materials. The utilization of microscopy plays a crucial role in the progression of human comprehension in several domains such as biology, materials science, medicine, and other related disciplines. (1)

Today, microscopy is used in many different contexts. It's a crucial instrument for researchers studying organisms and their inner workings, cells. Microscopic analysis of tissues and cells is fundamental to both the diagnosis of disease and the advancement of medical knowledge. To help in product development and quality control, material scientists rely on microscopic examinations of materials to determine their characteristics. Microscopy is essential for the study and manipulation of nanoscale materials in the field of nanotechnology. Microscopy is important in many fields, including chemistry, geology, environmental research, forensics, art conservation, and many more; it enables advances in technology, health, and scientific knowledge by providing critical insights across disciplines.

Light microscopy, electron microscopy, fluorescence microscopy, confocal microscopy, and scanning probe microscopy are some of the more frequent types of microscopies. Samples may be magnified and resolved with light microscopy, whereas electron microscopy makes use of electron beams to achieve greater resolution imaging. Fluorescence microscopy uses fluorescent markers to highlight

certain molecules, whereas confocal microscopy reduces stray light to provide clearer pictures. Atomic force microscopy and scanning tunneling microscopy are two types of scanning probe microscopy that enable nanoscale surface analysis.

In the scientific imaging method known as Confocal fluorescence microscopy, fluorescent molecules inside a sample are excited by a laser. As these molecules relax back to the ground state from the excited state, they produce light at certain wavelengths. In contrast to conventional fluorescence microscopy, however, this method makes use of a pinhole aperture to only collect light emanating from a single focus plane. Confocal fluorescence microscopy creates significantly crisper and sharper pictures of the focal plane of interest by removing out-of-focus light. This development allows for three-dimensional imaging by scanning at varying depths within the sample, which is useful for gaining a comprehensive perspective in a variety of fields, including biology and medicine.

In order to obtain high-resolution pictures of biological tissues and other materials, a new imaging technology known as optoacoustic microscopy (sometimes called photoacoustic microscopy or PA microscopy) combines the concepts of optics with acoustics (2). Using the light absorbed the object, researchers may observe its internal structures and characteristics. The sample is illuminated in optoacoustic microscopy with the help of a short-pulsed laser. The fast expansion and contraction of the sample material is caused by a temporary temperature increase produced when the laser light is absorbed by the sample. Ultrasonic waves (acoustic waves) are produced by this thermal expansion and travel into the tissue. Specialized transducers pick up on these acoustic waves and transform them into electrical signals that may later be processed into a picture. The capacity to get high-resolution pictures of tissues and structures at different depths, even in optically scattering mediums such as biological tissues, is one of the main benefits of optoacoustic microscopy. It's useful for functional imaging of blood arteries (3), cancers (4), and other biological characteristics since it provides strong contrast depending on the optical absorption properties of distinct molecules. Medical imaging, preclinical research, and even dermatology can all benefit from optoacoustic microscopy. It paves the way for the noninvasive visualization and investigation of tissues at depths that have so far been inaccessible using standard optical microscopy methods, facilitating both basic and clinical research.

Non-linear microscopy

In the fields of mathematics and science, a nonlinear system is a system in which the change of the output is not proportional to the change of the input. This is also sometimes referred to as a non-linear system. In a linear relationship, if one variable is doubled, the other one will increase proportionally. However, this simple proportionality is not present in nonlinear media.

NLM is an advanced imaging technique that takes advantage of the nonlinear optical properties of materials to attain high-resolution imaging in biological and material science applications. By utilizing the simultaneous absorption of two photons or second-harmonic generation, nonlinear microscopy offers enhanced depth penetration, reduced photodamage, and label-free imaging capabilities, making it a potent tool for obtaining detailed three-dimensional images in a variety of fields. (5) (6)

Single-photon excitation

In single-photon excitation, an atom, molecule, or semiconductor is excited by a single incident photon of the correct energy (wavelength). To excite a system from its ground state to its excited state, the energy of the photon must be equal to the energy gap between the two states.

Promoting an electron from the ground state to the excited state requires an interacting photon with an energy equal to the energy gap between the ground state and the excited state. Many other effects, such as the emission of light (fluorescence) upon the electron's eventual return to the ground state, are linked to this electron transition, which is commonly coupled with changes in the electronic configuration.

Two-photon excitation

Two-photon excited fluorescence, also known as TPEF, is a sophisticated optical microscopy technique that makes use of a nonlinear process. In this process, two photons with lesser energies, which are typically in the near-infrared range, interact with a fluorophore simultaneously to produce fluorescence in the fluorophore. When compared to the more traditional method of one-photon excitation, this procedure, which takes place at the focal point of a pulsed laser, enables three-dimensional

imaging of biological specimens to be performed with far less photodamage and greater depth penetration (6). By confining excitation to the focal plane, TPEF delivers improved spatial resolution by reducing the amount of background fluorescence produced by fluorescence that is out of focus. Because of its reduced auto- fluorescence, it is beneficial to biological study, especially in the fields of neuroscience and developmental biology. This makes it possible to conduct accurate analyses of cellular architecture, molecular interactions, and protein dynamics within living specimens.

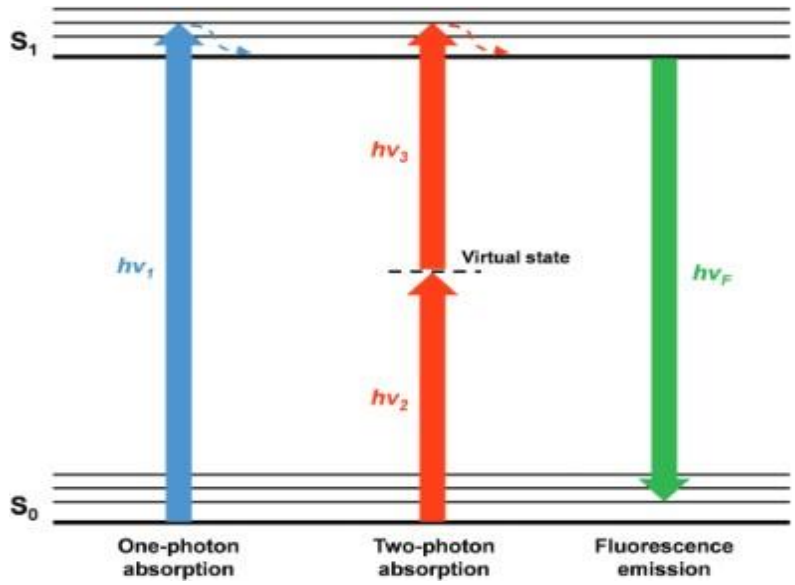

Figure 1 Energy diagram of one-photon and two-photon excitation. The fluorescence is emitted from the first electronic excited state regardless of the excitation mode. (7)

Second Harmonic Generation (SHG) is a nonlinear optical process in which two photons with the same energy combine within a nonlinear material, causing the emission of a photon with exactly twice the energy (half the wavelength) of the photons that were incident on the material. This photon has exactly half the wavelength as the incoming photons. Because this process takes place without the requirement for electronic transitions, it is ideally suited for imaging non-centrosymmetric structures such as collagen fibers seen in tissues. In contrast, two-photon excited fluorescence, also known as TPEF, is another nonlinear optical process. TPEF occurs when a fluorophore concurrently absorbs two photons with lower energies, which causes the fluorophore to release a photon with a higher energy level (fluorescence). The mechanisms and applications are the primary areas of differentiation between the two: SHG does not involve fluorescence or electronic transitions and is particularly useful for label-free imaging of structural components, whereas TPEF relies on fluorophores and is employed for cellular and

molecular imaging in biological samples. TPEF offers advantages in reduced photodamage, depth penetration, and three-dimensional resolution due to its nature as a multiphoton technique. SHG is particularly useful for imaging structural components.

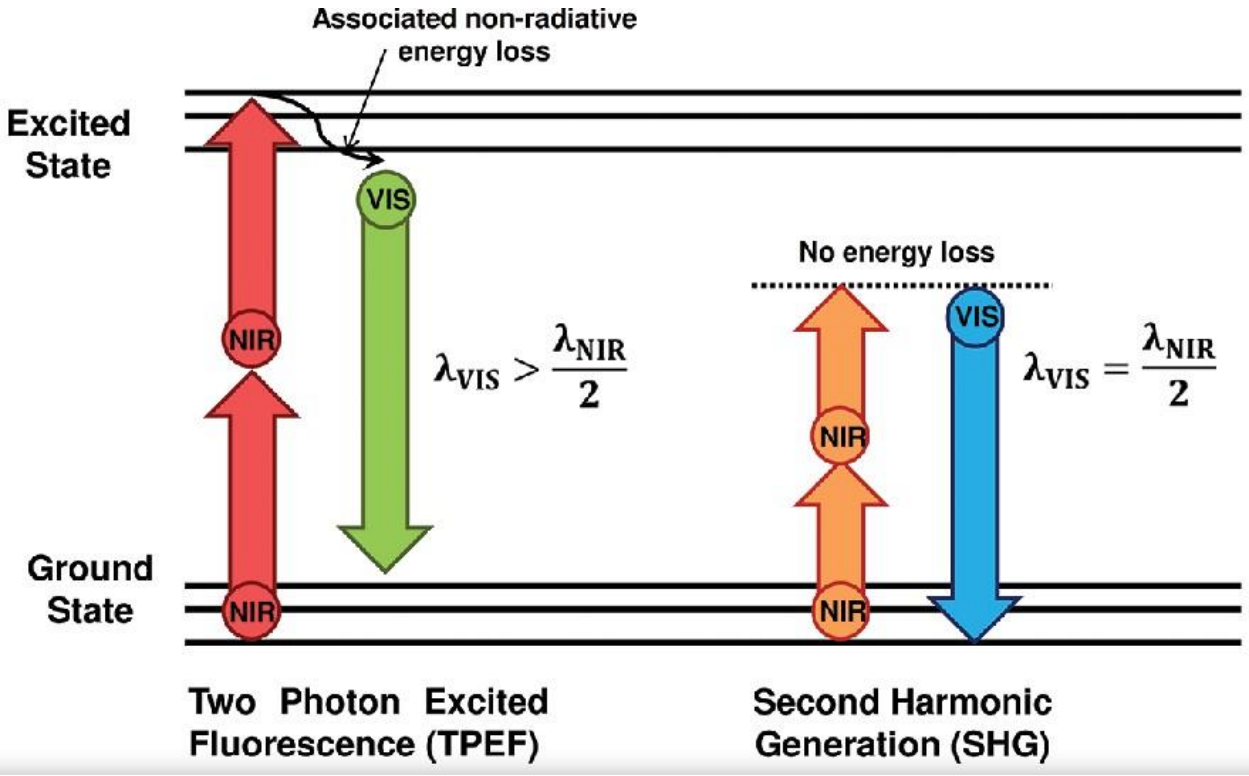

Figure 2 Jablonski energy diagram showing the process involved for two photon excited fluorescence (TPEF) and second harmonic generation (SHG). TPEF requires the existence of an actual excited state, while SHG does not. (8)

Laser Scanning Microscopy

Laser scanning microscopy is a sophisticated imaging methodology that utilizes laser illumination to acquire high-resolution, three-dimensional representations of

specimens. The system functions by utilizing a series of fundamental elements and principles. These include a laser light source that produces concentrated and coherent illumination, a scanning mechanism that systematically moves the laser beam across the sample, objective lenses of exceptional quality for accurate focusing and light collection, and detectors with high sensitivity to capture emitted or reflected light. Point-scanning microscopy involves the utilization of a laser beam that is concentrated into a minute point and systematically moved over the specimen. The light emitted or reflected from each individual point plays a role in the formation of the ultimate image. Confocal imaging is a widely employed technique in which a pinhole aperture is positioned in front of the detector to selectively eliminate out-of-focus light. This configuration allows for optical sectioning and enhances contrast in the resulting images. Laser scanning microscopy finds extensive application across many disciplines such as biology, materials science, and medicine. This technology facilitates the examination of cellular structures, live cells, tissue architecture, and other intricate samples, hence serving as a fundamental tool for scientific investigation and visualization and why it is the most used method. (9)

System characterization

Field Of View

The term "field of view" (FOV) in microscopy pertains to the observable region or segment of the specimen that is visually accessible through the optical system of the microscope during a specific instance. The measurement is commonly denoted in linear units, such as millimeters or micrometers, and signifies the breadth or magnitude of the area observable via the eyepiece or captured inside an image. The field of view (FOV) is subject to various parameters, such as the type of objective lens employed, the level of magnification applied by the microscope, and the dimensions of the detector or camera sensor. Typically, objectives with higher magnification tend to yield smaller fields of view (FOVs), whereas objectives with lower magnification tend to produce broader FOVs. In the field of microscopy, scientists and experts frequently make deliberate selections about the suitable objective lens and magnification level. These choices are made by considering the precise demands of their observations, while also considering the trade-off between achieving a high level of magnification and ensuring that an adequate portion of the sample is captured within the field of view.

In other words, the concept of field of view in an image pertains to the overall range of the image field that can be observed simultaneously. There is frequently a tradeoff between field of view and spatial resolution. As an illustration, the act of "zooming in" with a camera result in a trade-off between the field of view and the level of resolution.

Spatial resolution

The spatial resolution of a microscope pertains to its ability to differentiate and resolve intricate features in an image by determining the minimum distance between two separate points or structures within the examined object. The primary determinants of this phenomenon encompass various aspects, such as the wavelength of the imaging light, the numerical aperture of the objective lens, the quality of optical components, sample preparation processes, detector sensitivity, and microscopy techniques. The importance of spatial resolution in microscopy cannot be overstated, as it determines the extent to which fine details may be observed and studied. This capability allows researchers to examine complex structures and phenomena in biological, materials, and various other samples with a high degree of accuracy and distinctness.

Group delay dispersion

Group delay dispersion (GDD), commonly referred to as group velocity dispersion, is a fundamental characteristic in the field of optics, specifically in relation to ultrafast laser systems. This phenomenon pertains to the variation in the velocities of light of different wavelengths when they propagate through optical materials or components. In the context of ultrafast laser applications, whereby pulses of extremely short duration are employed, the consideration of group delay dispersion (GDD) becomes paramount importance due to the potential for pulse broadening or distortion resulting from dispersion effects. Researchers and engineers possess the ability to manipulate and enhance the temporal characteristics and waveform of ultrafast laser pulses for various purposes such as laser micro processing, multiphoton microscopy, and high-speed data communication. This is achieved through the management of Group Delay Dispersion (GDD) utilizing specialized optics or dispersion compensation techniques. When correcting for GDD we want to estimate where the maximum signal (fluorescence) is received to obtain most detailed image possible.

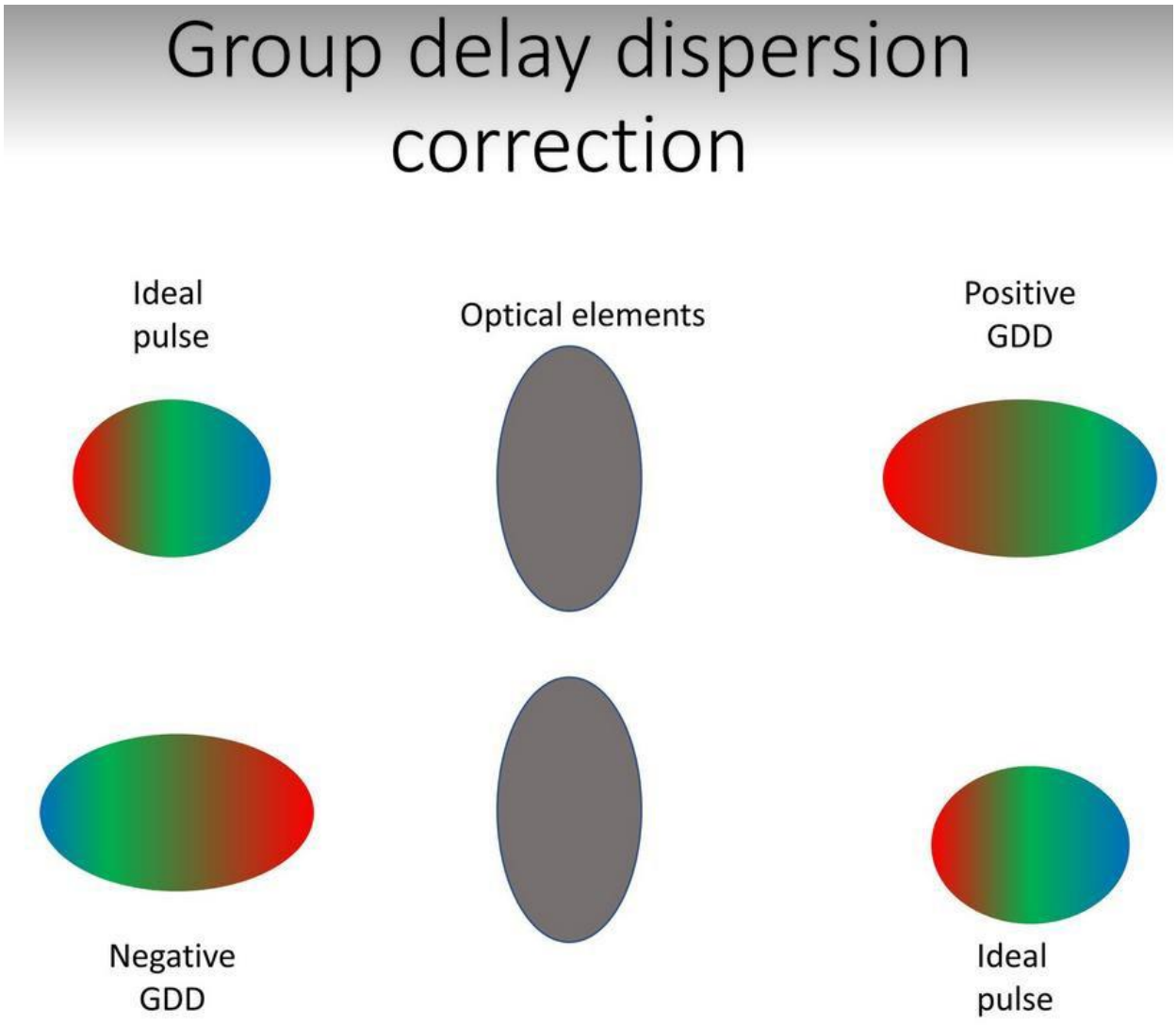

Figure 3 A rough representation of the effects of GDD on the ultra-short laser pulses.

The fundamental concept of GDD correction is to provide a "negative" group delay, in which the "blue" wavelengths precede, so that the resulting pulse after passing through the optics is more ideal. Our optical elements induce a positive delay, which gives a greater phase velocity to shorter wavelengths resulting in a more stretched out pulse. By giving a negative GDD we give a head start to longer wavelengths so that at the end the pulse is closer to ideal. It is important to have short compact pulses in order to maximize photon density and by extension the probability of simultaneous photon absorption.

Materials and methods

Non-linear microscopy imaging setup

In this section of this thesis, we will discuss the materials and methods used in order to obtain the best final result.

Below is a general set up used for the acquisition of NLM. It consists of a laser source that generates a coherent beam, two galvanometric mirrors that scan the beam along the x and y axes, a dichroic mirror that reflects or transmits specific wavelengths of light, an objective lens that focuses the coherent beam on the sample, and a photon multiplier unit that amplifies the signal received and transmits it to the computer.

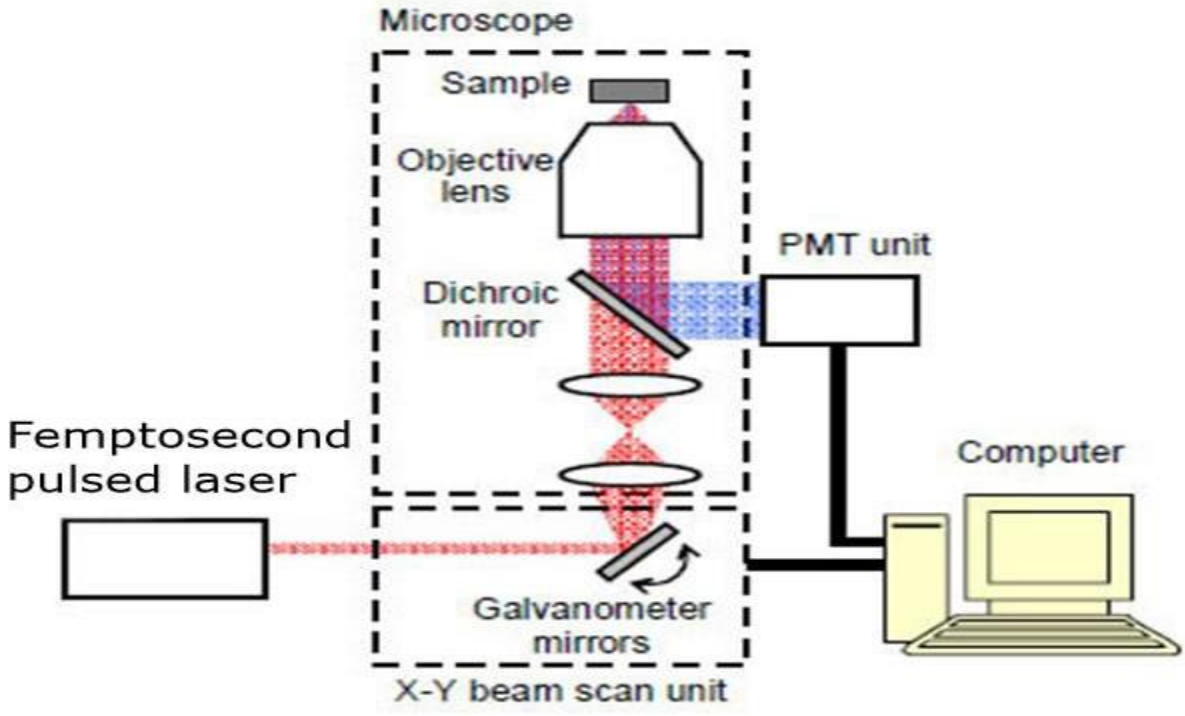

Figure 4 NLM imaging setup using an ultra-fast puled laser similar to the one used in our laboratory. (10)

Field Of View

To quantify the field of view of the captured images on the computer screen, an analysis was conducted on microscope images of a starch sample, specifically corn flour. The objective of this experiment is to adjust the position of the microscope stage, which is the component responsible for holding the sample, to align the two crystals with the outermost boundaries of the viewing area. In a more specific manner, I documented the precise locations of two crystals that were enclosed within the starch sample and recorded their exact positions in micrometers (μm). The laser wavelength used was 900nm. The precise visual representations are as follows:

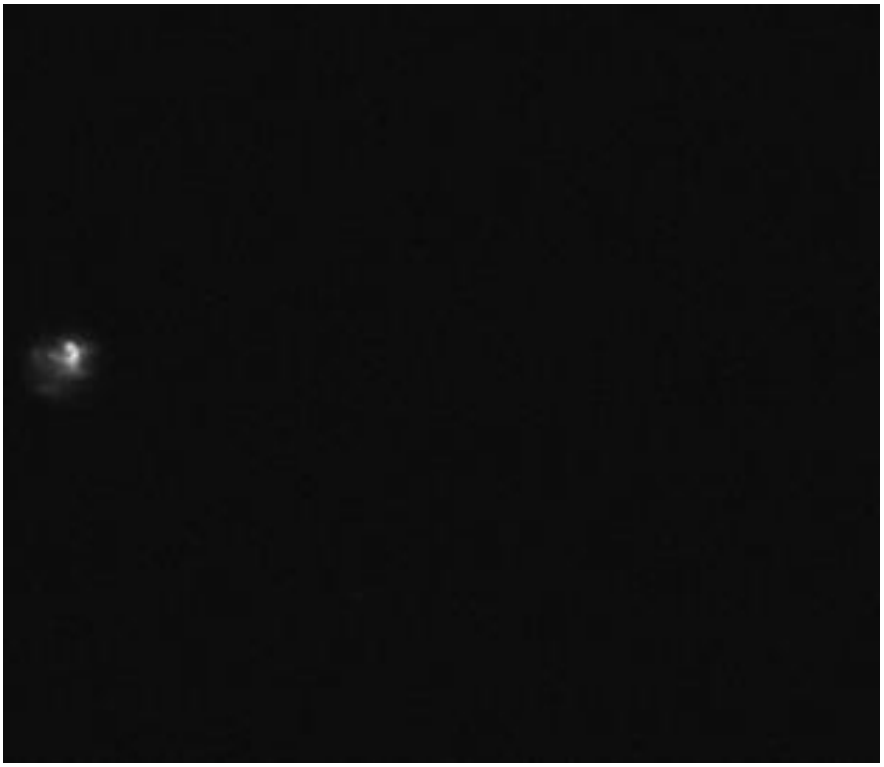

Figure 5 Corn flour crystal moved to the left side of the computer screen . Precise position measured at 3798μm.

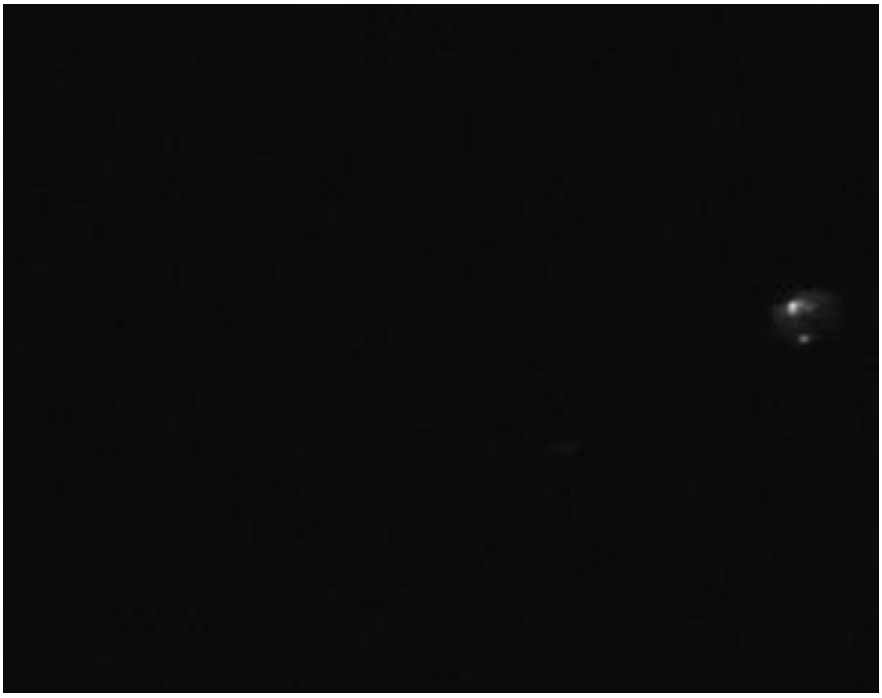

Figure 6 Corn flour crystal moved to the right side of the computer screen**.** Precise position measured at 3638 μm.

With the assistance of ImageJ, I merged the two images together as shown below:

Figure 7 The two channels highlighted and merged in a single image. 3798μm. (Blue) 3638 μm (Green).

The objective of this study is to acquire the signal profile of the most prominent spots on two crystals, with the intention of afterwards quantifying the distance between these peaks in terms of pixels.

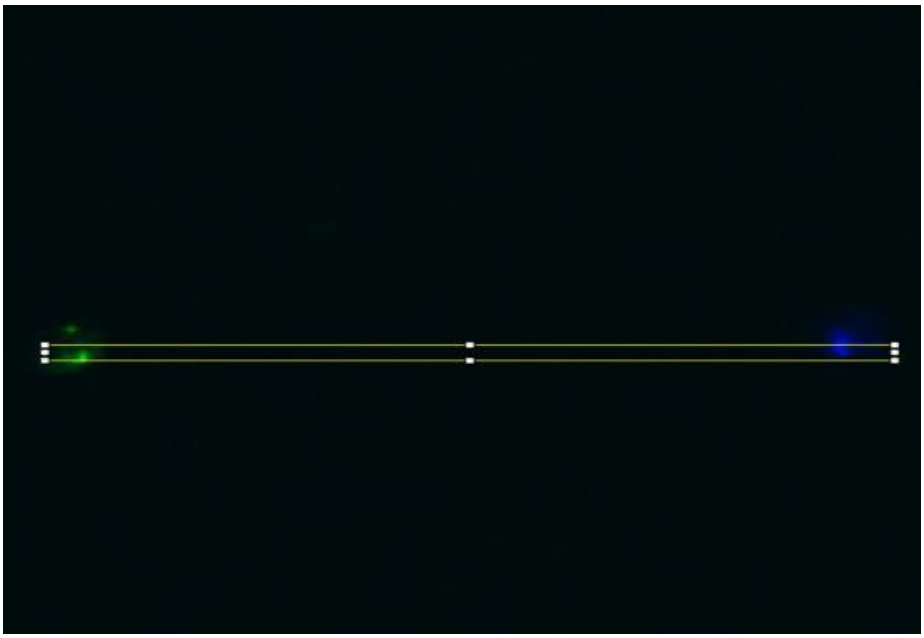

Figure 8 The area covered by the rectangle will be represented in an Intensity (Gray value) vs distance(pixels) graph by ImageJ.

Below you will find the signal profile obtained:

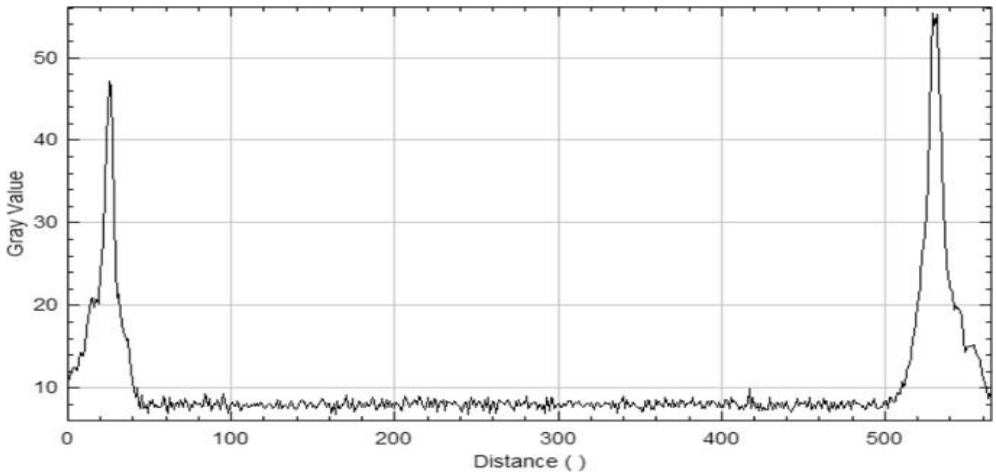

Figure 9 This is the resulting signal profile covered by the rectangle.

After acquiring the signal profile, our objective is to ascertain the precise location of each peak. The achievement of this task involves the application of two Gaussian functions to accurately model each peak. Origin subsequently provides us with the exact pixel coordinates.

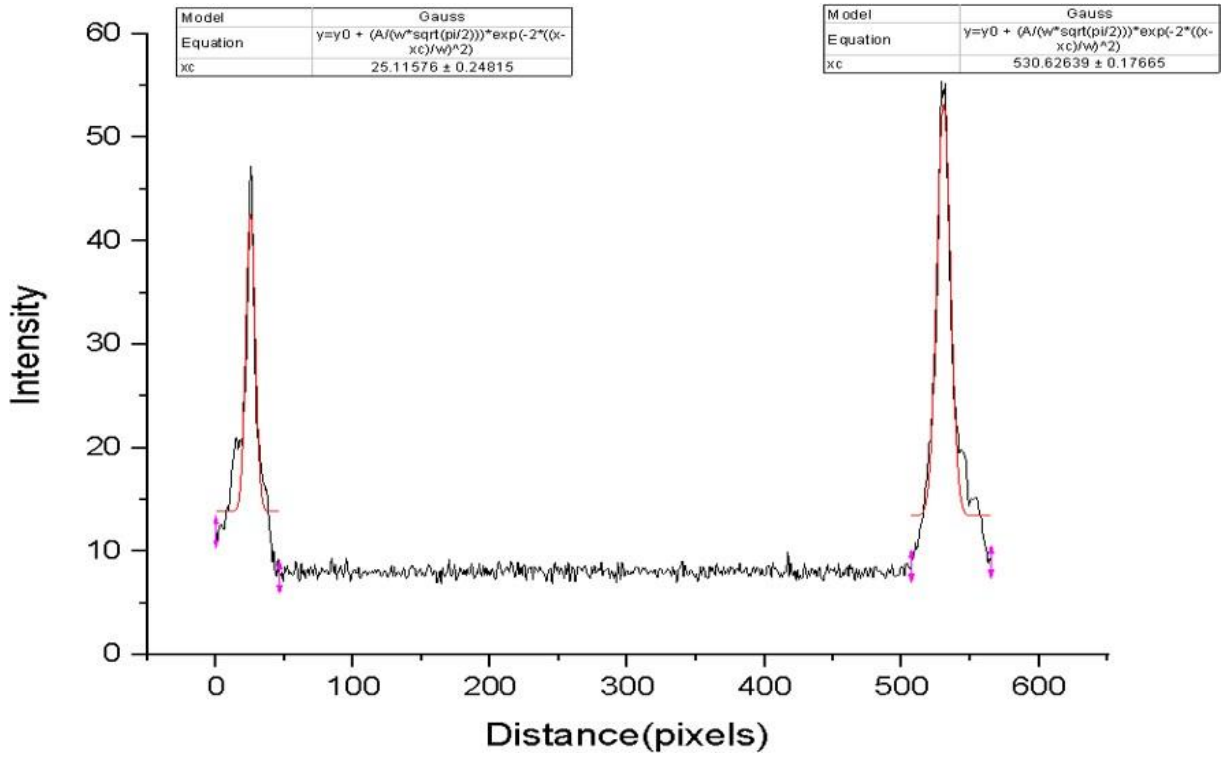

Figure 10 The signal profile imported in Origin for the estimation of each peak position.

Measurement of the pixel size

*The initial measurement yielded a value of 3798 μm.

*The second measurement yielded a value of 3638 μm.

*The distance between the two crystals is measured at 160 μm.

*The pixel size is calculated by dividing 160 micrometers by 505.5 pixels, resulting in a value of 0.316 micrometers.

*The field of view of the image has been determined.

Spatial resolution

To assess the spatial resolution of the image, a sample including minuscule spherical shapes with a diameter of 500nm is employed, while a wavelength of 900nm is used once again to obtain the image. After capturing the image on the computer screen, set the scale on ImageJ to the pixel size that was measured earlier. it is necessary to choose the smallest viewable sphere in order to ensure that the FWHM remains below the diffraction limit.

Figure 1 Image of sample containing small fluorescent spheres on the computer screen. The arrow points to the sphere that was used for the determination of the spatial resolution.

Once we have zoomed in to the point where the individual pixels are visible, we acquire the signal profile of the smallest sphere.

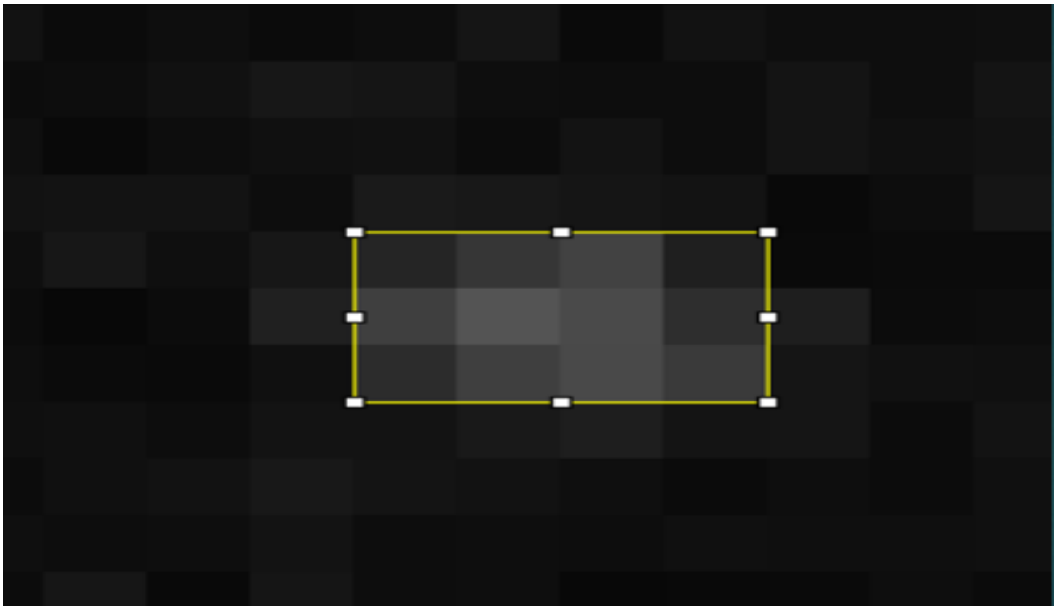

Figure 12 Image of the zoomed in sphere. The rectangle indicates the area chosen for signal acquisition.

Using the same procedure of Gaussian fitting as before we obtain:

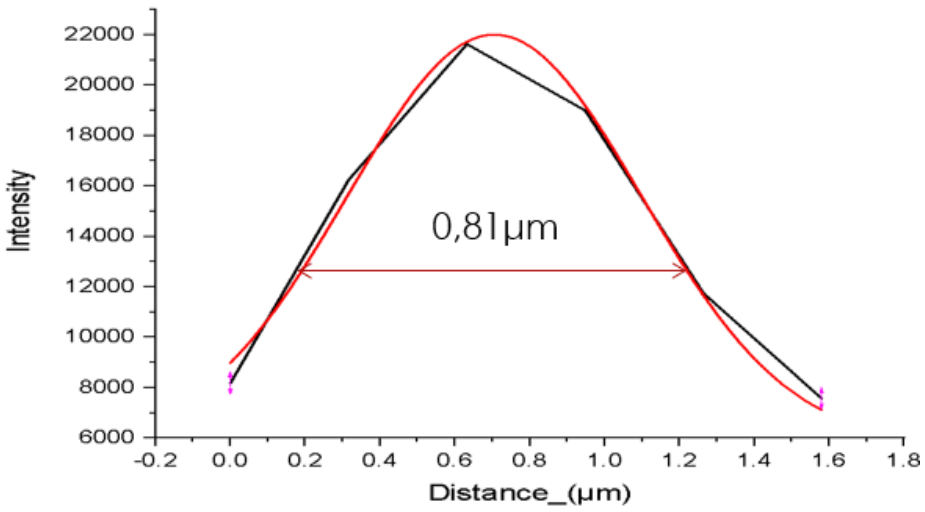

Figure 13 Gaussian fit on the signal peak of the smallest sphere detectable.

FWHM is used to quantify how diffuse an imaging system's response is to point sources. It's a helpful metric for judging spatial resolution because it's directly related to the system's capacity to resolve small details. If the FWHM is less, it means the system can discriminate between more closely spaced items, indicating higher spatial resolution.

In this case with a pixel size of 316 nm, FWHM is measured at 810nm. Any optical instrument or system, such as a microscope, telescope, or camera, has a fundamental resolution limitation in optics due to the mechanics of diffraction. If an optical instrument has attained this resolution limit, it is said to be diffraction limited. Other factors may affect an optical system's performance, such as lens imperfections or aberrations, but these are caused by errors in the manufacture or calculation of a lens, whereas the diffraction limit is the maximum resolution possible for a theoretically perfect, or ideal, optical system. (11)

The angular resolution of an instrument, in radians, is proportional to the wavelength of the observed light and inversely proportional to the diameter of its objective's entrance aperture. The size of the smallest diffraction-limited image feature for telescopes with circular apertures is the size of the Airy disk. As one reduces the aperture size of a telescopic lens, diffraction increases proportionally. Due to the Abbe diffraction limit, it is challenging to observe sub-wavelength structures through a microscope. Ernst Abbe discovered in 1873 that light with wavelength lambda traveling through a medium with refractive index n and converging to a point with half-angle theta has a minimum resolvable distance of

$$D = \frac{\lambda}{2nsin\theta} = \frac{\lambda}{2NA} \quad (12)$$

Where NA is the numerical aperture of the objective lens.

Using that formula given that the numerical aperture of the objective lens we used (neofluar) is 0.7 we can calculate the theoretical values of spatial resolution.

This process was repeated for a variety of wavelengths resulting in the following graph:

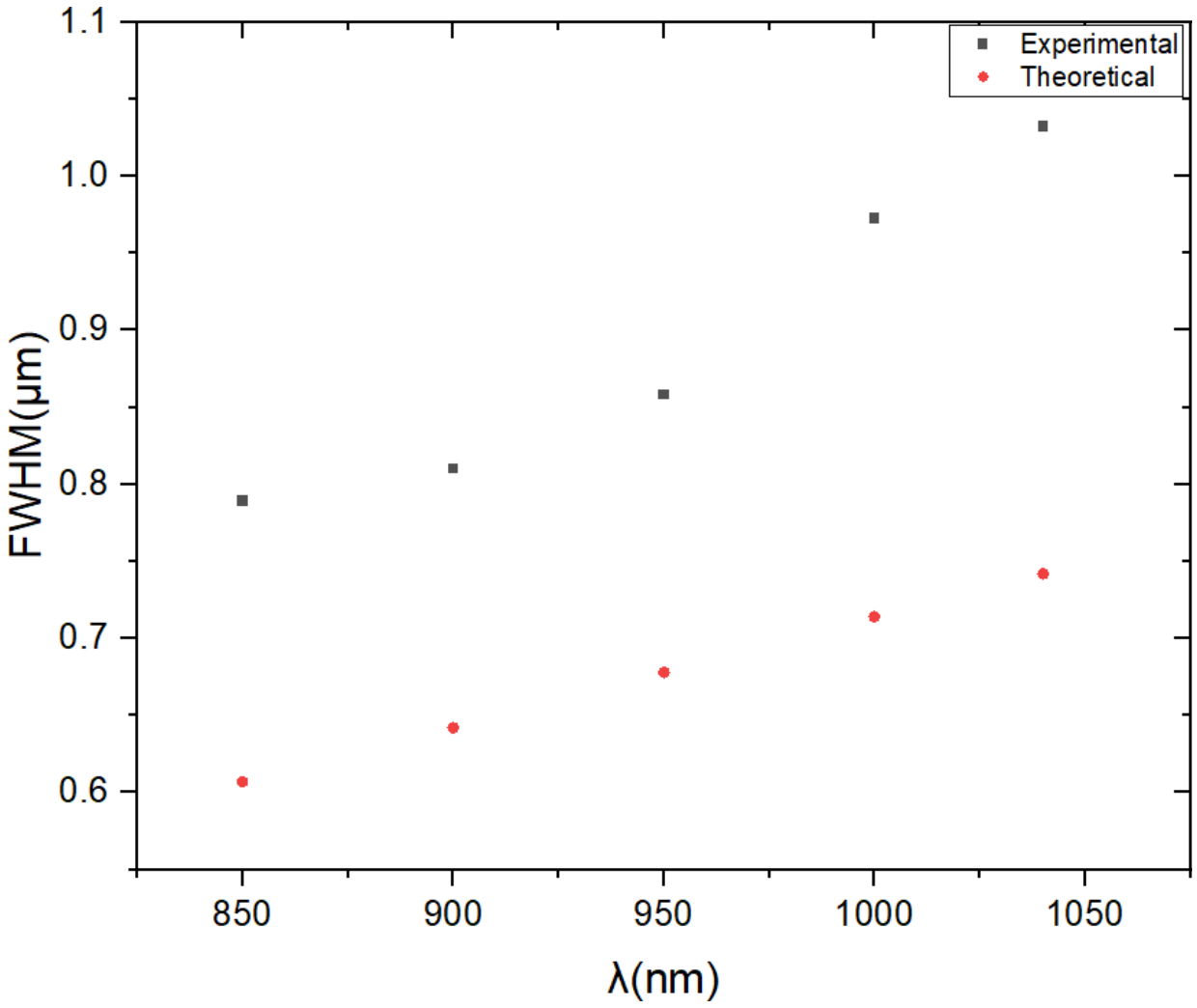

Figure 14 Graph illustrating the behavior of spatial resolution in response to different wavelengths, with the theoretical values calculated by Abbe's diffraction limit formula.

Group Delay Dispersion

To determine the optimal adjustment for Group Delay Dispersion (GDD) for a particular wavelength, I conducted measurements of fluorescence intensity for each image corresponding to varying wavelengths, while manipulating GDD values.

Presented below are two graphs showcasing the relationship between GDD and intensity at varying wavelengths correspondingly:

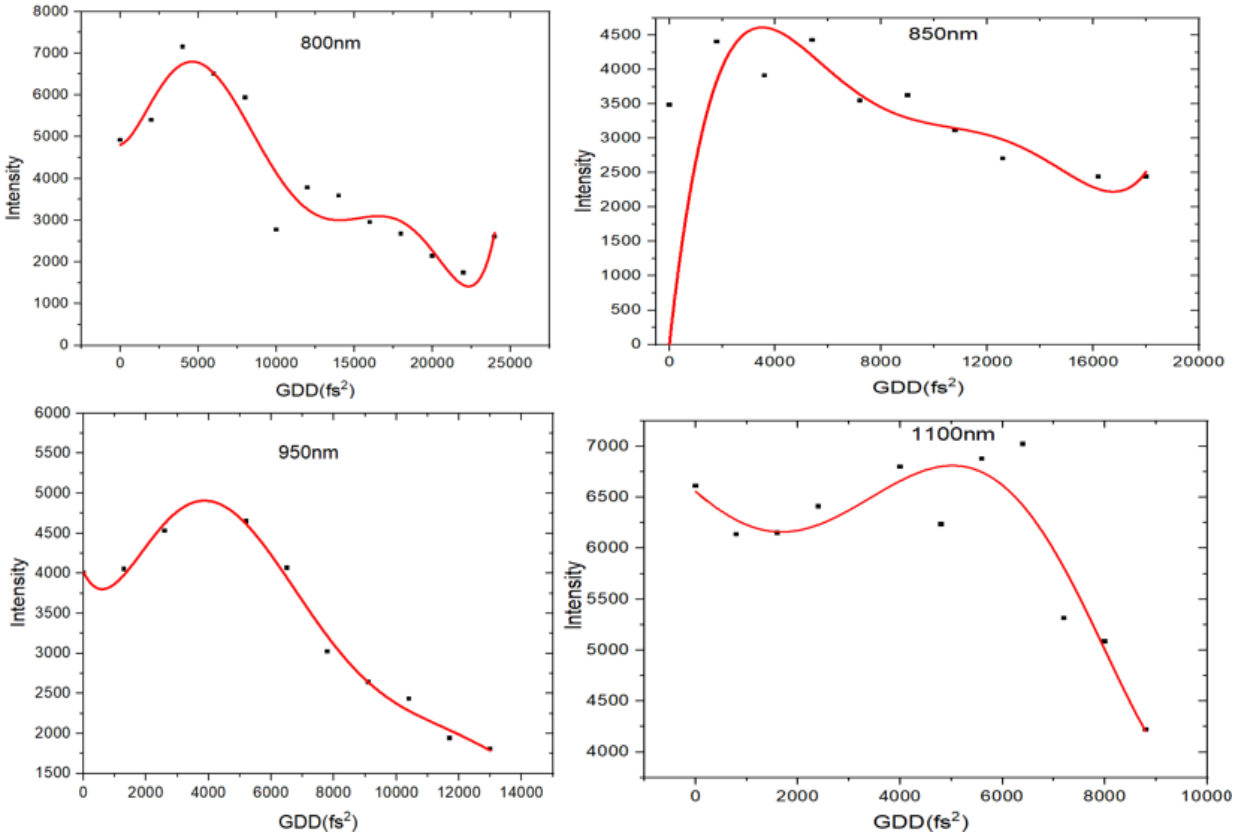

Figure 15 Graph illustrating the behavior of Group Delay Dispersion in response to different wavelengths.

As shown above, the dispersion of light through the optical system appears to be heavily dependent on the wavelength used prompting us to adjust the correction for Group Delay Dispersion accordingly.

To estimate the GDD correction corresponding to the maximum light intensity I created the following graph.

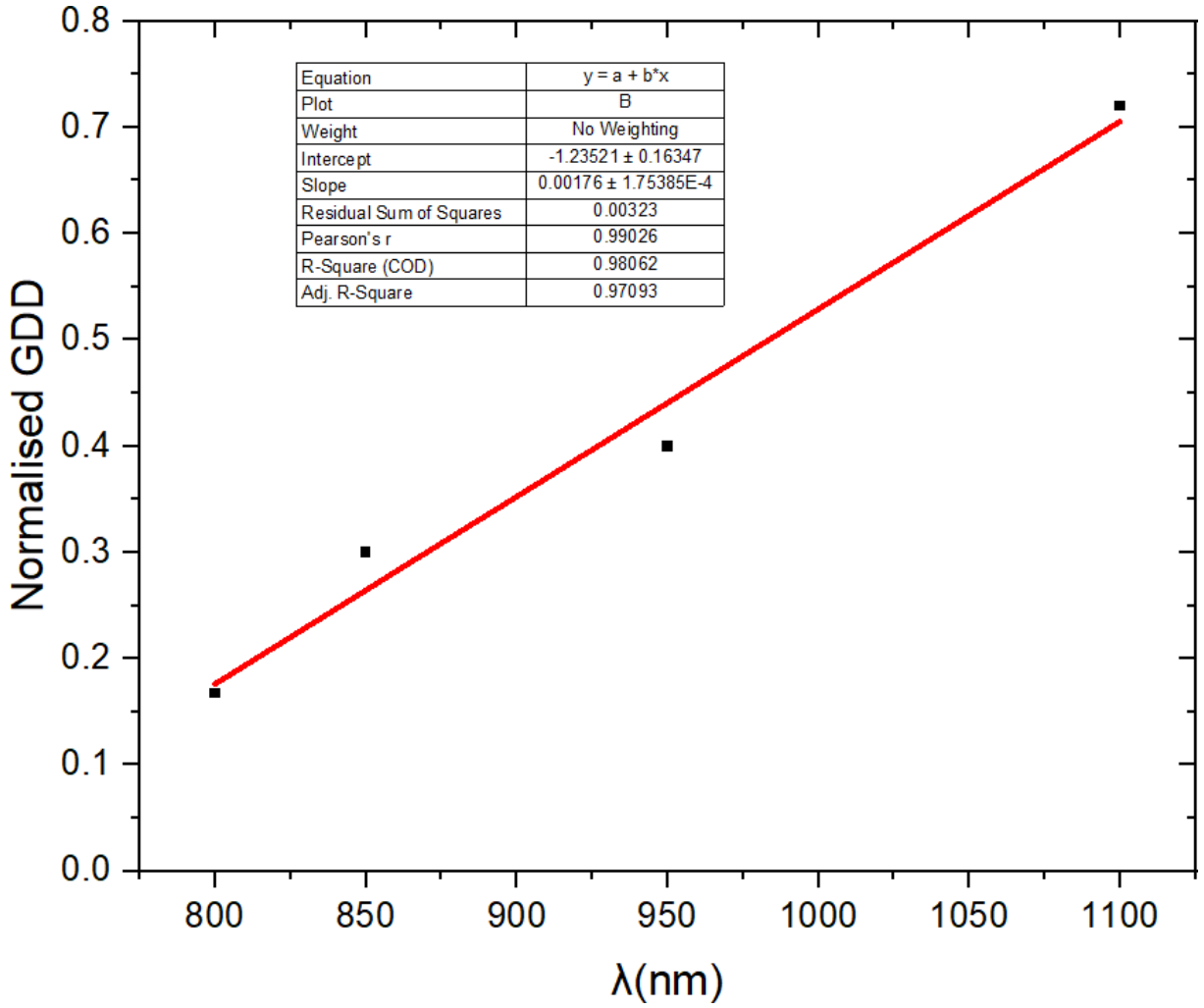

Figure 16 Linear relationship between Normalized correction for GDD and wavelength.

Where Normalized GDD = $\frac{GDD_{peak}}{GDD_{max}}$ where the numerator refers to the correction for GDD corresponding to the maximum Intensity and the denominator to the maximum value of GDD correction used.

The graph indicates a clear linear relationship between correction and wavelength. Moreover, this linear fit enables us to make predictions regarding the location of the maximum point for any given wavelength, eliminating the need for measurement.

Results

After this long preparation we are finally able to examine the images obtained from the laboratory microscope, pertaining to the behavior of different biological probes such as dsRed and DAPI, as well as retinol powder which is a form of Vitamin A. The end result is the demonstration of the entire retina for the three different mechanisms, Autofluorescence, TPEF, SHG. The process we followed to acquire the following results was to scan different images of each sample in different wavelengths. After that to search for the brightest spot in each image and use ImageJ to calculate the mean Intensity for each image.

The intensity-wavelength diagram for the following chromophores comprises a crucial element of our study. The latter are depicted in the following Figures. A clear understanding of the absorption and emission characteristics of these samples is important to fully grasp its significance in the biological processes investigated within this thesis.

dsRed

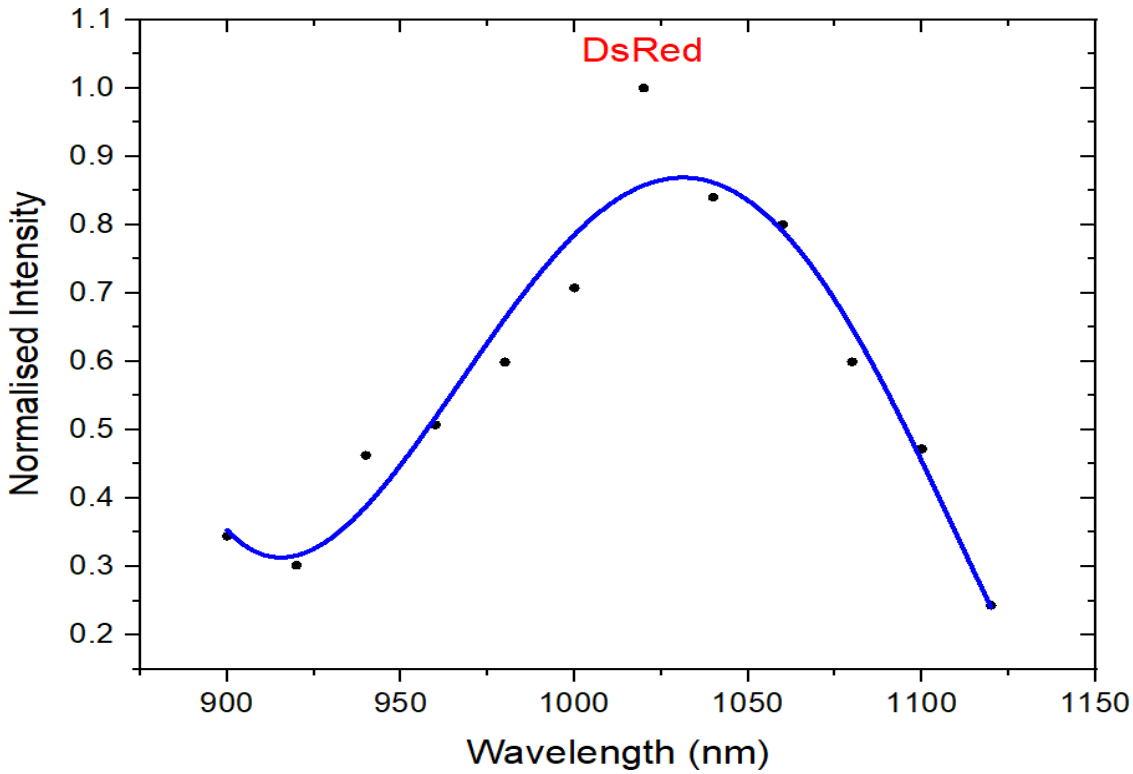

Figure 18 Fluorescence of dsRed in the spectral range of (900-1120) nm. For the clear illustration of its mathematical behavior a fifth order polynomial fit was used.

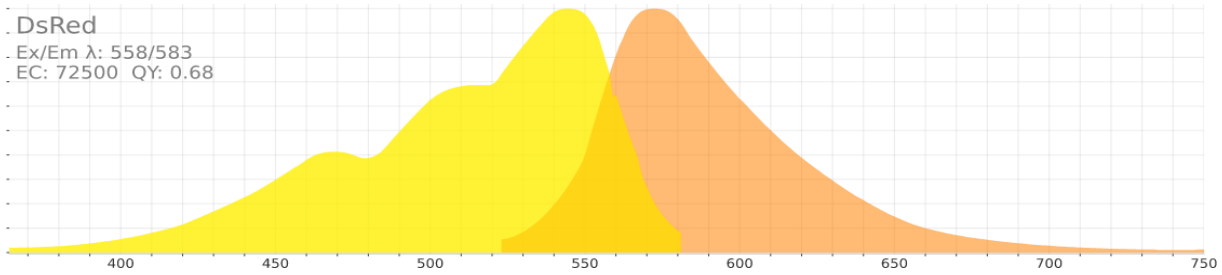

Figure 19 Excitation and emission curve overlap of dsRed. Image generated using (13).

The maximum fluorescence signal from dsRed, was measured at an excitation wavelength of 1020 nm (Figure 18) during Two-Photon Excited Fluorescence, showing it is consistent with the principles of TPEF, since the fluorescence wavelength of dsRed for single-photon excitation is 558nm (7).

This result highlights the advantages of TPEF, such as reduced photobleaching and enhanced penetration depth, which make it suitable for deep tissue imaging. The selection of a 1020 nm excitation wavelength aligns with these benefits, assuring effective and less damaging excitation of dsRed, which is especially advantageous for examining biological samples and enabling imaging studies with minimal photodamage. Dividing the maximum wavelength for TPEF by 2 we obtain the respective experimental single photon excitation wavelength for dsRed. Comparing theoretical and experimental values for single photon we observe a Blueshift from 558nm→510nm.

Based on the above diagram, it can be shown that the intensity of dsRed exhibits a parabolic form. The observed phenomenon reveals an apparent decrease in intensity as the distance from the peak at 1020nm increases.

Below I present the respective image obtained through our microscope:

DAPI

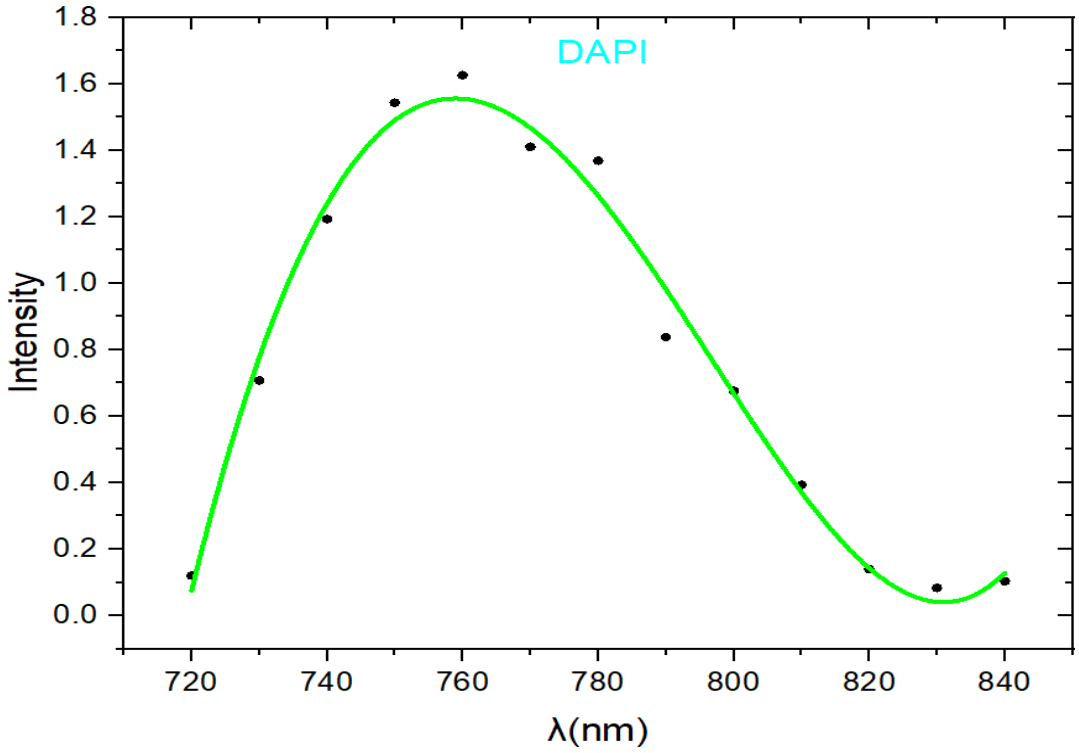

Figure 21 Behavior of DAPI fluorescence in the spectral range of (720-840) nm.

Like dsRed, DAPI exhibits a parabolic form as well only this time the parabola is much narrower resulting in more abrupt decrease in intensity. The maximum fluorescence signal from DAPI, was measured at an excitation wavelength of 760 nm (Figure 21) during Two-Photon Excited Fluorescence, showing it is consistent with the principles of TPEF, since the fluorescence wavelength of DAPI for single-photon excitation is 359 nm (8). Dividing the maximum wavelength for TPEF by 2 we obtain the respective experimental single photon excitation wavelength for DAPI. Comparing theoretical and experimental values for single photon we observe a Redshift from 359nm→380nm.

The Figure below illustrates the absorption and the emission curves for DAPI in single photon fluorescence:

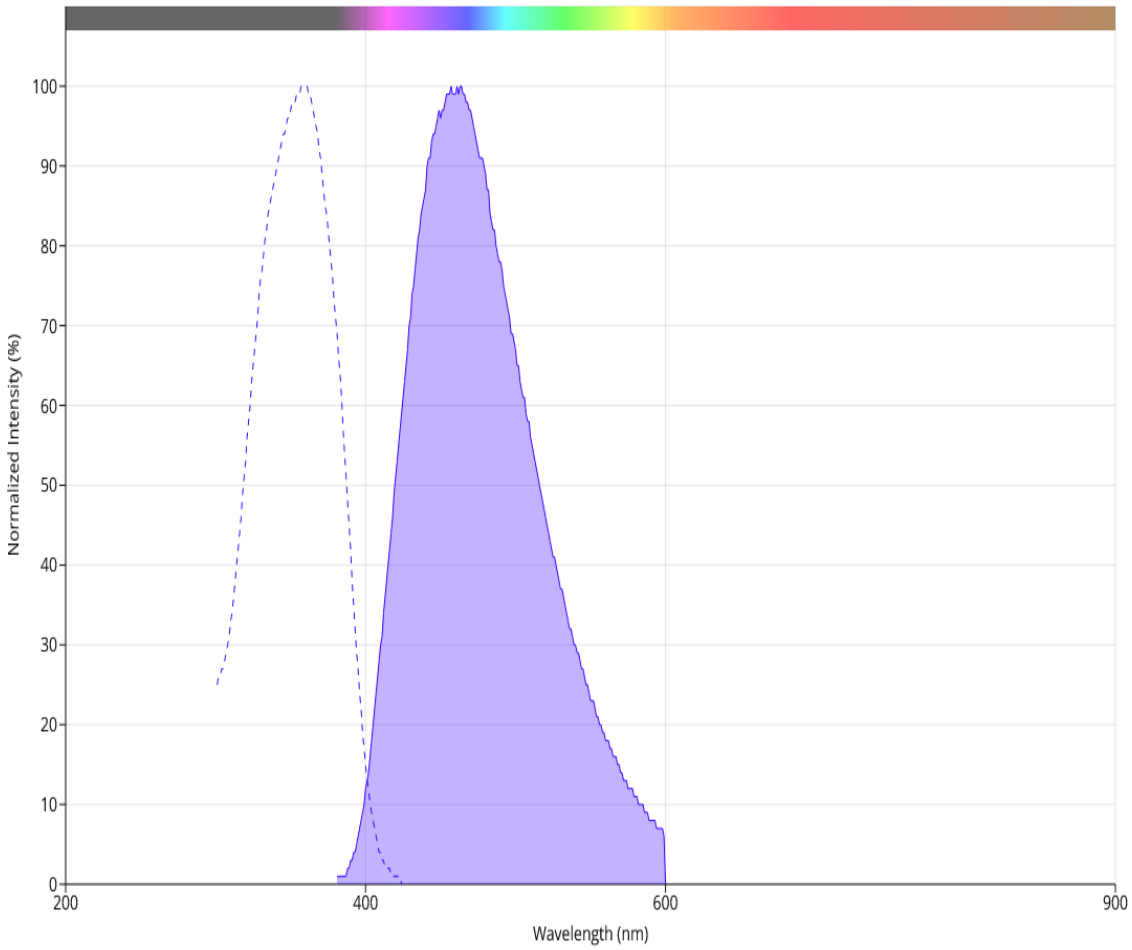

Figure 22 Image showcasing the single photon excitation peak of DAPI. Appearing at 359nm. Image generated using (14).

Dividing the maximum experimental wavelength for TPEF by 2 we obtain the respective experimental single photon excitation wavelength for DAPI. Comparing theoretical and experimental values for single photon we observe a Redshift from 359nm→380nm.

Below I present the respective image of mouse retina cell nuclei painted over by DAPI corresponding to the maximum fluorescence wavelength:

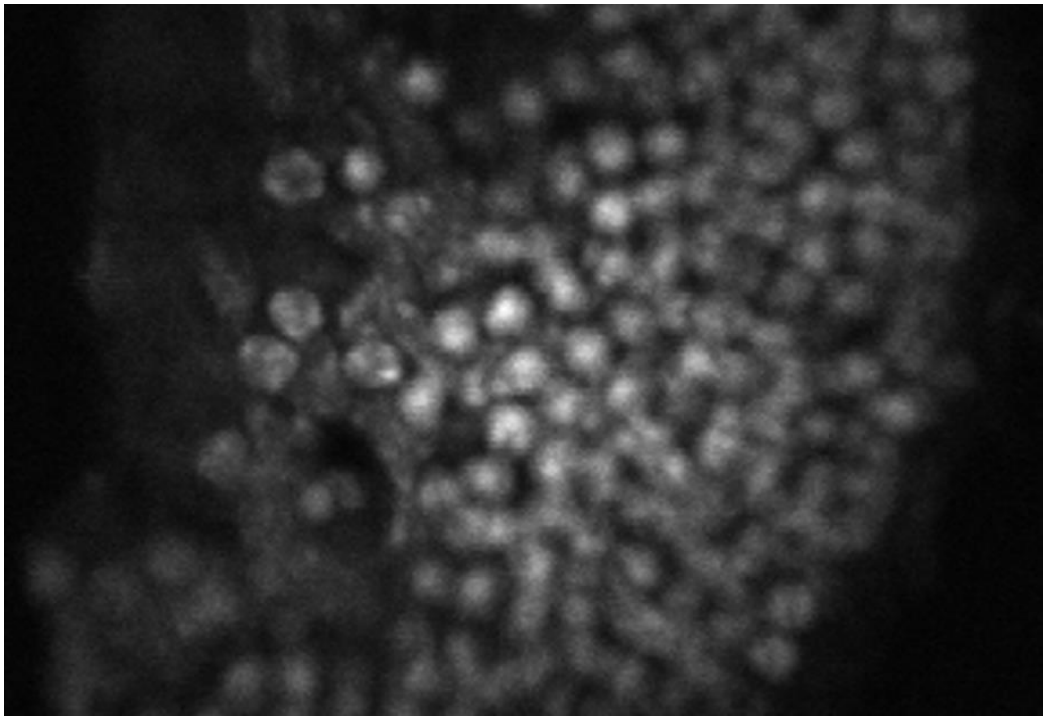

Figure 23 Mouse retina cell nuclei covered by DAPI**.** Image generated using the maximum fluorescence wavelength at 760nm.

Retinol

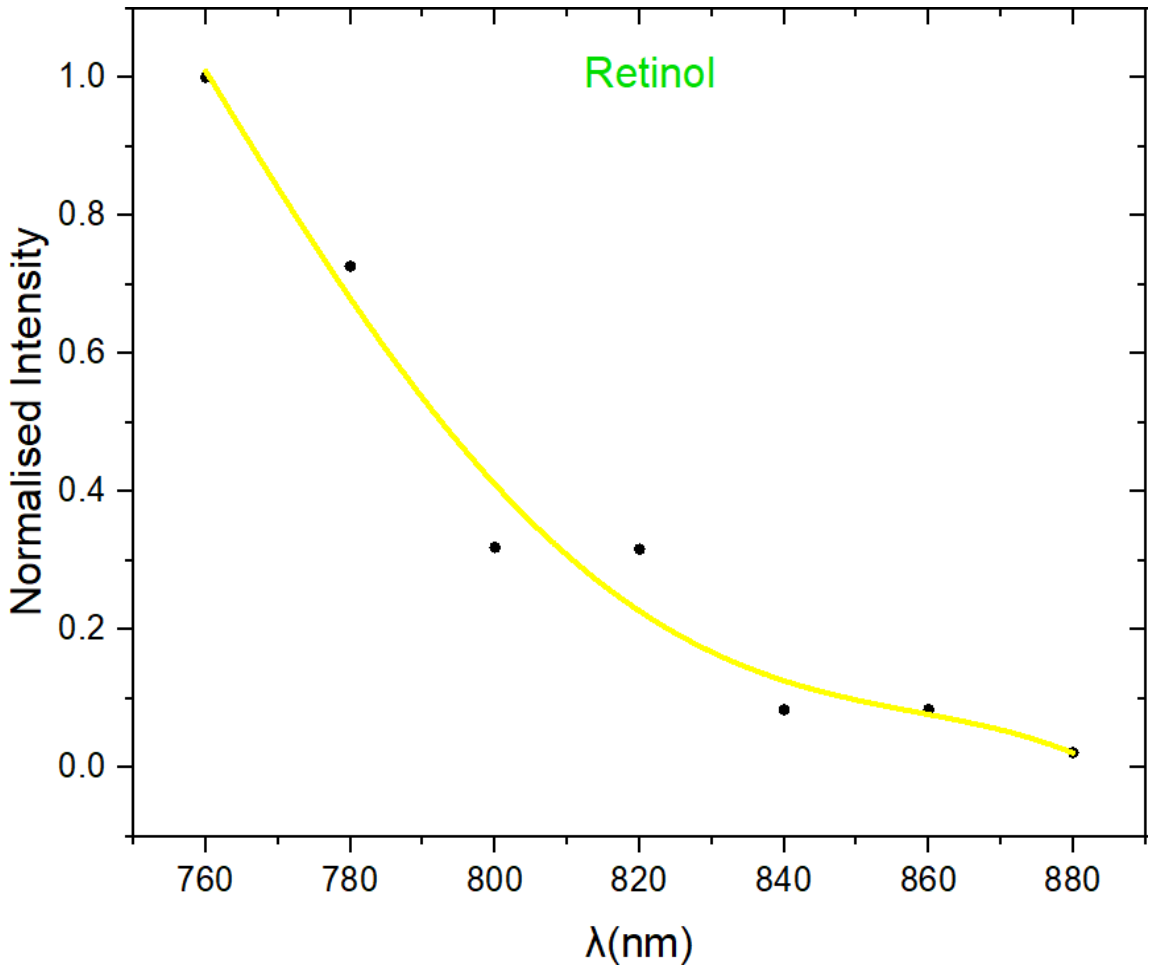

Figure 24 Behavior of retinol fluorescence in the spectral range of (760-880) nm.

In the case of retinol (Vitamin A) the maximum fluorescence signal was measured at a wavelength of 760nm with the single photon value being at 335nm (15). Once again this implies that the measurement acquisition for TPEF was successful and within the expected range, thus providing all the associated benefits.

In Figure 24 I showcase the downward trend of retinols fluorescence in response to the spectral range we can obtain clear sample images.

We observe Redshift from 355nm→380nm.

For wavelengths below 760nm our microscope was unable to receive fluorescent signal from the sample. This was likely due to the dichroic mirror blocking wavelengths close to 700nm and below.

Below I present the image of maximum intensity for retinol as observed from the lab computer screen:

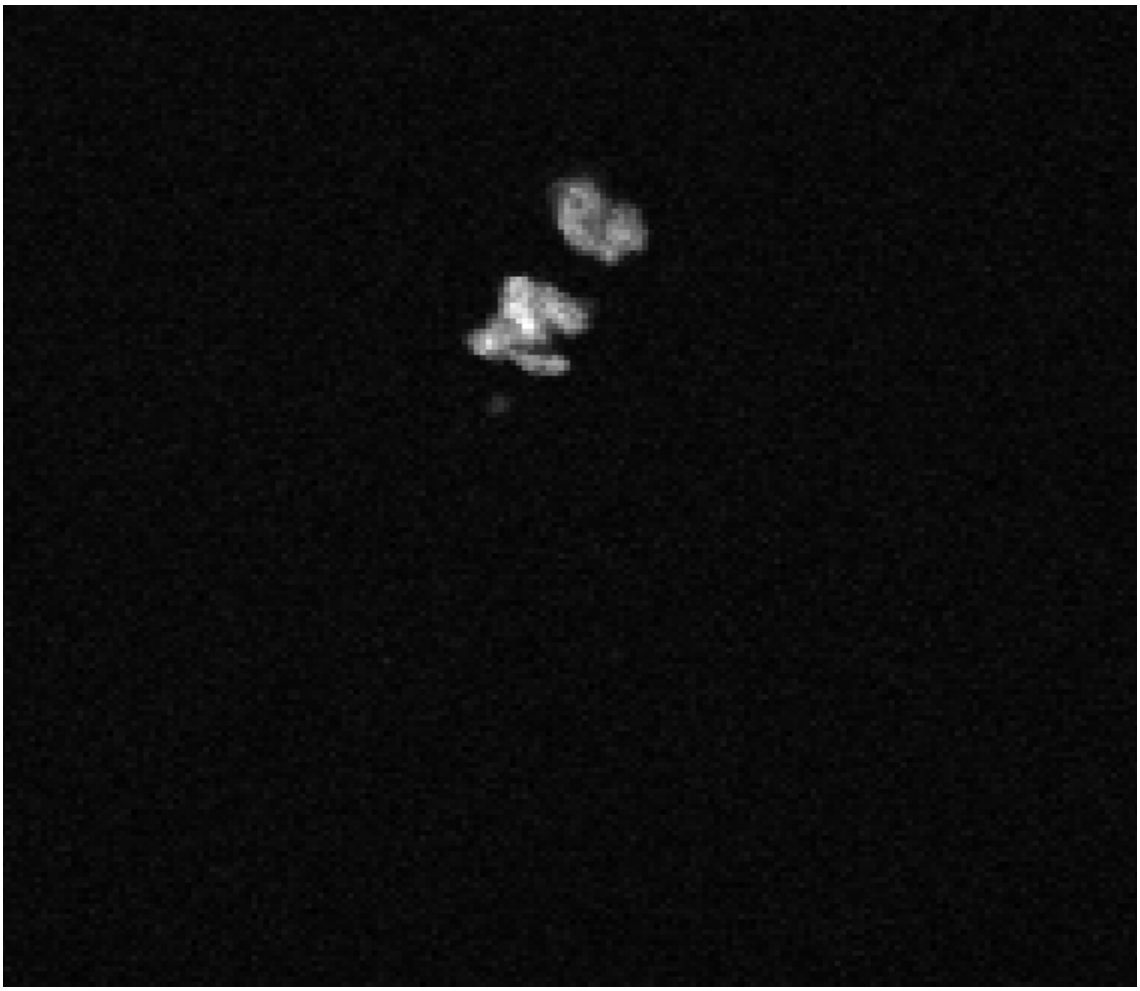

Figure 25 Image of retinol powder corresponding to the maximum fluorescence intensity at 760 nm.

Mouse retina tissue

For the final part of this project, I used a mouse retina tissue that was removed from a mouses eye and rolled out in the shape of a strip. After that the cell nuclei of the retina were painted on by the previously mentioned chromophore DAPI. The purpose of this was to examine the response of the tissue to varying wavelengths of light. We found that for different wavelengths there was a different corresponding natural mechanism. The three observed (Figure 26) were TPEF for DAPI, autofluorescence and SHG with the respective images shown below:

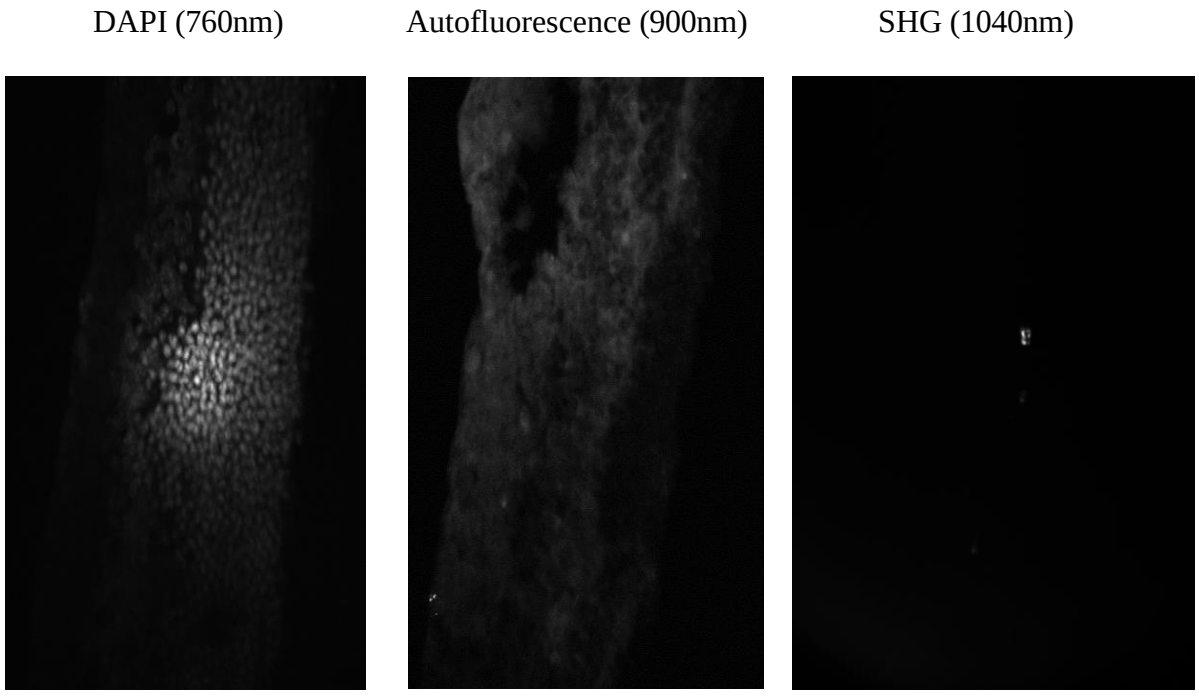

Figure 26 The three different mechanisms corresponding to different images. Each image is a small fraction of the entire retina for a different wavelength. I collected a total of 15 images for different positions of the retina for each wavelength.

In the first image, the cell nuclei that were covered by DAPI are clearly visible, but not in the other two images. As shown in Figure 21 DAPI fluoresces maximally at a

wavelength of 760nm which was consequently the one used to acquire the first image in Figure 23 aiming to obtain the best image possible. However, as showcased by Figure 21, the wavelengths of 900nm and 1040nm are outside the spectral range of fluorescence for DAPI so it makes sense that we get no image of the cell nuclei. What we do get however is autofluorescence which is the fluorescence of the entire retina, (with the exception of course of the cell nuclei), and SHG for wavelengths of 900nm and 1040nm respectively. It is clear that we don't receive nearly as much signal from SHG compared to the other two mechanisms, and the reason is because centrosymmetric molecules, like the ones contained inside the retina, produce light that interferes destructively. Due to the molecule's symmetry light waves maintain a constant phase that causes this interference. For example, for greater signal output we could use tissues rich in non-centrosymmetric molecules like collagen for instance. Such an example is regular muscle tissue.

Complete retina images

The final step of this project was to try to stitch all 15 of the retina images collected at different positions, to get a full picture of what we are looking at. To achieve this, I used a plug-in program called MosaicJ which then allowed me to manually stitch the 15 images together with the use of ImageJ. With the added feature of ImageJ I was able to manipulate the overall brightness of the individual images to achieve a more homogeneous final appearance. The three images presented in Figure 27 are the result of the manual stitching of the individual parts of the retina, (like the ones shown in Figure 26), resulting in an approximation of the actual retina.

The finished product is showcased below:

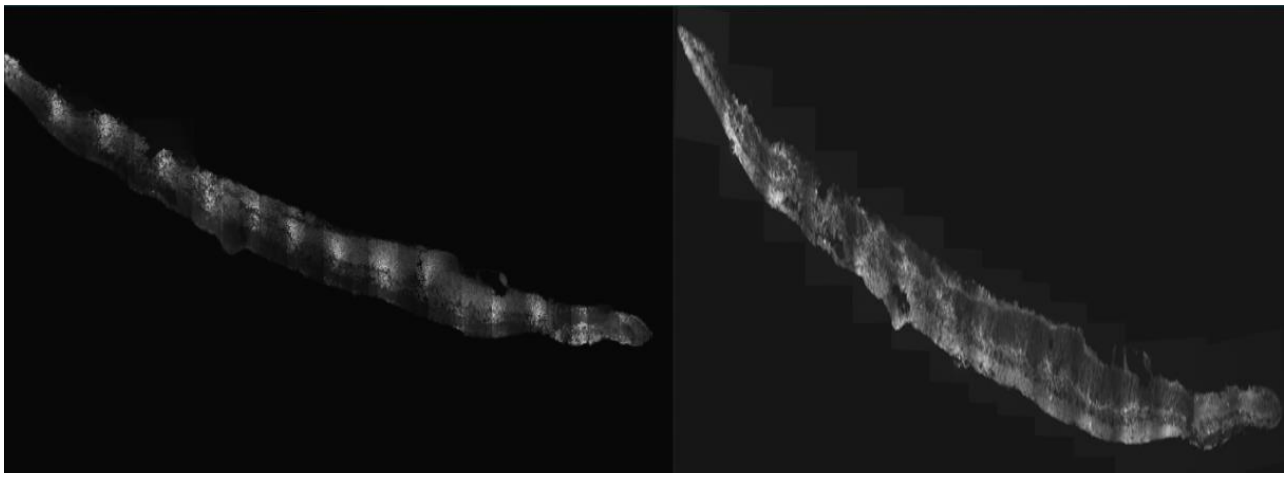

Figure 27 End result. The entire retina in response to autofluorescence and TPEF. The Image is a result of manual stitching using MosaicJ.

The absence of the SHG stitched retina is due to the absence of signal in many of the individual images.

Conclusions

In the case of correction for GDD we conclude that by acquiring value corresponding to the maximum intensity compared to the uncorrected value we observe the following increases in intensity for each wavelength:

Wavelength (nm)	Increase in Fluorescence(%)
800	45
850	28
950	16
1100	9

By the linear fit for Normalized GDD vs wavelength we conclude that by the value of the slope we can predict future measurements without the need for laboratory measurements.

For the spatial resolution values there is a clear discrepancy from the theoretical values. The reason for this is likely poor laser beam quality resulting in an imperfect pulse as well as due to aberrations of our optical elements, resulting in wider peaks and by extension greater FWHM values.

For the different substances we found the wavelength of maximum fluorescence by plotting the measured mean intensity values with respect to wavelength.

samples	**Maximum fluorescence wavelength(nm)**
retinol	760
dsRed	1020
DAPI	760

Keeping these results in mind I used these laser light wavelengths to obtain the images for this thesis. It is important to note here that all the values we obtained are within the expected range when compared their single photon excitation equivalent. This successfully illustrates the benefits of NLM such as reduced photobleaching and enhanced penetration depth due to the longer wavelengths used, which make it suitable for deep tissue imaging.

Bibliography

1. https://www.abebooks.co.uk/9780195162608/Handbook-Biomedical-Nonlinear-Optical-Microscopy-0195162609/plp

2. http://dx.doi.org/10.1038/nmeth.1483

3. https://www.sciencedirect.com/science/article/abs/pii/S1053811917300587

4. https://pubmed.ncbi.nlm.nih.gov/33057275/

5. https://www.sciencedirect.com/book/9780123694706/nonlinear-optics

6. https://www.nature.com/articles/nbt899

7. Wu, L., Liu, J., Li, P., Tang, B., & James, T. D. (2021). Two-photon small-molecule fluorescence-based agents for sensing, imaging, and therapy within biological systems. *Chemical Society Reviews*, *50*(2), 702-734.

8. Thomas, G., Voskuilen, J.V., Gerritsen, H., & Sterenborg, H.J. (2014). Advances and challenges in label-free nonlinear optical imaging using two-photon excitation fluorescence and second harmonic generation for cancer research. Journal of photochemistry and photobiology. B, Biology, 141, 128-38.

9. https://www.ncbi.nlm.nih.gov/pmc/articles/PMC4863715/

10. Taira, K., Hashimoto, T., & Yokoyama, H. (2007). Two-photon fluorescence imaging with a pulse source based on a 980-nm gain-switched laser diode. *Optics Express*, *15*(5), 2454-2458.

11. Born, Max; Emil Wolf (1997). *Principles of Optics*. *Cambridge University Press*. *ISBN 0-521-63921-2*.

12. *Lipson, Lipson and Tannhauser (1998). Optical Physics. United Kingdom: Cambridge. p. 340. ISBN 978-0-521-43047-0.*

13. https://www.fpbase.org

14. https://www.aatbio.com.

15. Futterman, S., Swanson, D., & Kalina, R. E. (1975). A new, rapid fluorometric determination of retinol in serum. *Investigative ophthalmology*, *14*(2), 125-1